In Vitro Transepithelial Drug Transport by On-Line Measurement: Cellular Control of Paracellular and Transcellular Transport

PETER R. WIELINGA,[†] ESTHER DE WAAL,[†] HANS V. WESTERHOFF,[‡] AND *JAN LANKELMA*[*,†,‡]

Contribution from *Academisch Ziekenhuis Vrije Universiteit, Department of Medical Oncology, P.O. Box 7057, Room BR232, 1007 MB Amsterdam, The Netherlands; and BioCentrum Amsterdam, Vrije Universtiteit, Department of Molecular Cell Physiology, De Boelelaan 1087, 1081 HV Amsterdam, The Netherlands.*

Received December 28, 1998. Final revised manuscript received August 19, 1999.
Accepted for publication September 21, 1999.

Abstract □ Studies on transcellular transport across epithelial cell layers are performed mostly by discontinuous sampling of the transported compound. This has several drawbacks, e.g., it gives disturbances in volume, it limits the time-resolution, and is often laborious. In this report we introduce a method to measure transepithelial transport of fluorescent compounds continuously. The time-resolution is at the (sub)minute scale, allowing the measurement of the change in transport rate before and after transport modulation. We will describe how we used the method to measure transcellular and paracellular transport. For highly membrane-impermeable compounds, the paracellular transport and the regulation of the tight junctions was studied in wild-type and MDR1 cDNA transfected epithelial canine kidney cells (MDCKII). The effect of the multidrug transporter P-glycoprotein (Pgp) on the transepithelial transport was studied. Addition of the Pgp inhibitor SDZ PSC 833 showed a modulation of the idarubicin (IDA) and daunorubicin (DNR) transport, which was larger during transport from the basolateral to the apical side than in the reverse direction. By modeling the transepithelial transport, we found that in these cells Pgp had more effect on the basolateral to apical transport than vice versa, which can be attributed to a relatively large passive permeation coefficient for the cellular basolateral plasma membrane.

Introduction

Compartmentalization is important for multicellular organisms' functioning, so that the different biochemical tasks necessary for life are performed in the proper place under the proper conditions. The barriers between such compartments are often such that only regulated biochemical transport and communication can take place between the different compartments. Examples of such barriers are the epithelial cells in the gut and the endothelial cells of the blood−brain barrier.[1−4] Characteristic for these cell layers is that a-specific transport can hardly take place, due to the architecture of these layers. Tight junctions connect neighboring cells firmly to each other and hardly leave any (paracellular) space between the cells. Thereby a barrier is created with high transepithelial electrical resistance (TER) that is highly impermeable for most hydrophilic compounds.[5−8] Specific transporters and carriers regulate the transport of this class of compounds across these barriers.[6,8] For lipophilic compounds, which are able to passively diffuse across the cellular plasma membrane, epithelia and endothelia are often equipped with specialized proteins that regulate the transcellular transport (through the cells) of this class of compounds. An important example of such a transporter is P-glycoprotein (Pgp)[9−11] which functions as an ATP-dependent multispecific cellular drug efflux pump. Pgp was discovered as a transmembrane protein that induced cellular multidrug resistance (MDR),[11] i.e., resistance against several different anticancer drugs, e.g., daunorubicin (DNR), vincristine, taxol. However, not only are some anticancer drugs substrates, but many other types of compounds also interact with Pgp, e.g., cardiac drugs (verapamil, diltiazem), immunosuppressors (cyclosporins) and anti-AIDS drugs.[12,13] Epithelia and endothelia, with MDR1 Pgp localized in their apical plasma membrane, are found at several strategic sites in the body. Examples of such sites are the endothelial cells of the blood−brain and the blood−testes barrier and the epithelial cells lining the gut, where Pgp mediates drug transport out of the brain, the testes, and the body, respectively.[13−16]

Much knowledge on transepithelial transport has come from in vivo studies. However, ethical constraints limit the type of experiments that can be conducted in vivo. Also, because of the complexity of the multicellular organisms, it is often difficult to pinpoint which phenomena are related to specific molecular processes. In vitro models simulate the in vivo situation and do not have these drawbacks. Until now transepithelial transport has been measured discontinuously in time, mainly by measuring either the amount of substrate (mostly radioactively labeled, or fluorescent) transported from the apical to the basolateral (A to B) side of the cells (or vice versa) or by measuring the TER.[17−20] By combining knowledge of the study of MDR,[21,22] the use of fluorescence for detection, and the experience in developing in vitro techniques,[23,24] we developed a technique that can be used to study transepithelial transport continuously. The method makes use of commercially available plasticware and a fluorometer, equipment present in most biochemical laboratories. The method detects the transport of fluorescent substrates on-line, it has a high time-resolution, and effects of transport modulators can be studied within one experiment, thereby reducing the number of parameters that may give rise to errors.

With the method we successfully studied transepithelial transport in several different cell lines (Caco-2, LLC-PK1, and MDCKII). Here we describe how the technique is performed, and we report results obtained with the epithelial Madin−Darby canine kidney cell line MDCKII. We applied the method to carry out two types of experiments: (1) experiments in which the regulation of the tight junction is studied and (2) experiments in which the control of Pgp on the transepithelial transport is studied. Using a 70 kDa plasma membrane-impermeable fluorescein isothiocyanate-

* Corresponding author. Phone: +31-20-444 2603; fax: +31-20-444 3844; e-mail: J.Lankelma@azvu.nl.
[†] Academisch Ziekenhuis Vrije Universiteit.
[‡] BioCentrum Amsterdam.

10.1021/js980497z CCC: $18.00
Published on Web 11/11/1999

labeled dextran (FITC-dextran) or the highly negatively charged organic anion calcein (Cal), the paracellular transport (through the space between the cells) was studied, both in the wild-type MDCKII cells and the MDR1 cDNA transfected MDCKII-MDR1 cells. The influence of Pgp on the transcellular transport (involving the plasma membrane) was studied in the MDCKII-MDR1 using the membrane-permeable, fluorescent anticancer drugs daunorubicin (DNR) and idarubicin (IDA). While highly similar in chemical structure, these anthracyclines differ in their lipophilicity and membrane permeability, with IDA being more lipophilic than DNR. For both DNR and IDA, the transport from the basolateral to the apical (B to A) compartment and vice versa (A to B) and the effect of Pgp inhibition were studied. A drug transport model was developed to explain the differences in kinetics that were observed.

Experimental Section

Chemicals—Verapamil (Vp), diltiazem (Dil), calcein (Cal), fluorescein isothiocyanate labeled dextran (FITC-dextran) (MW = 70 kDa), 2-deoxy-D-glucose (deoxyglucose), and digitonin were obtained from Sigma (St. Louis, MO). DNR and IDA were from Farmitalia Carlo Erba (Brussels, Belgium). SDZ PSC 833 was obtained from Novartis (Basel, Switzerland). Cell culture media and supplements were obtained from Flow (Irvine, UK), and culture plastics from Nunc (Roskilde, Denmark). Fetal calf serum (FCS) was from Gibco (Paisley, UK), 4-(2-hydroxyethyl)-1-piperazine ethanesulfonic acid (HEPES) was from Serva (Heidelberg, Germany), and sodium azide (NaN_3) and ethylenediaminetetraacetic acid (EDTA) were from Baker Chemicals (Deventer, The Netherlands). Sodium penicillin G was from Yamanouchi (Leiderdorp, The Netherlands), and streptomycin sulfate was from Radiumfarma-Fisiopharma (Italy). Microporous polycarbonate membrane inserts (transwell No. 3413) with a pore size of 0.4 μm and a diameter of 6.5 mm were from Corning Costar (Badhoevedorp, The Netherlands). Plastic fluorescence cuvettes were from Falcon (Leiden, The Netherlands).

Cell Culture and Media—MDCKII cells, wild-type and MDR1 cDNA transfected (MDCKII-MDR1),[25] were obtained from Drs. Evers and Borst (NKI, The Netherlands) and cultured as previously described.[18] Cells were cultured in a cell incubator in humidified air (supplemented with 5% CO_2) at 37 °C, in DMEM with 20 mM HEPES (pH 7.4), supplemented with 7.5% heat-inactivated FCS, and penicillin (0.05 mg/mL) and streptomycin (0.1 mg/mL). For the transepithelial transport experiments, the cells were seeded on transwell membrane inserts (transwell vial) at 2500 cells/mm,^{2} and the medium was refreshed every day. Confluency of the cell monolayer on the microporous membrane was monitored by measuring the transepithelial electrical resistance (TER) using a Millicell electrical resistance meter (Millipore). On the basis of this measurement, the cells could be used for transport assays between day 3 to 6, when TER values were between 600 and 300 $\Omega \cdot mm^2$ and approximately $80-90 \times 10^3$ cells were present on the microporous membrane.

Experimental Setup—A transwell vial with cells grown to confluency was placed in a fluorescence cuvette. To fit a transwell vial (Costar), the cuvette was composed of a well of a 24-well polystyrene plate (Costar) placed on top of a polystyrene fluorescence cuvette (Falcon). A square, with the inner measurement of the cuvette, was taken out of the bottom of the 24-well plate well, creating a free opening between the cuvette and the well (see Figure 1). The cuvette was placed in a thermostated cuvette holder equipped with a magnetic stirrer, the latter situated under the cuvette holder. After each experiment the cuvette was cleaned and sterilized with ethanol for reuse. The medium in the lower compartment (cuvette) was stirred with a Teflon-coated magnetic stirrer bar. The medium in the upper compartment (transwell vial) was stirred with a small Teflon stirrer, attached to a small 24 V electric motor. The motor was attached to a metal plate with a free space fitting the top of the cuvette (see Figure 1). This ensured that the motor was placed properly. The Teflon stirrer speed was controlled at 100–150 rpm. During the experiments 3100 μL medium was present in the cuvette and 250 μL in the transwell

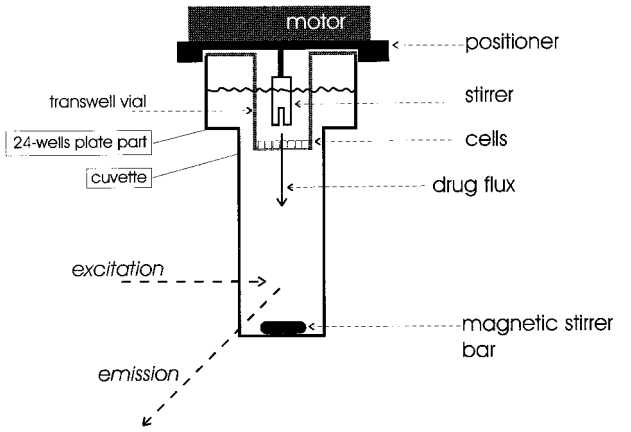

Figure 1—Schematic drawing of the experimental measurement setup. The cuvette used for the transepithelial experiments was composed of two parts: (1) a 24-well plate well on top of (2) a plastic fluorescence cuvette. The medium in the cuvette had a volume of 3100 μL and that in the transwell vial 250 μL. A Teflon stirrer driven by a 24 V electric motor stirred the medium in the transwell vial and a magnetic stirrer bar that in the cuvette. Transepithelial transport was monitored by measuring the fluorescent substrate (added to the transwell vial) that appeared in the cuvette.

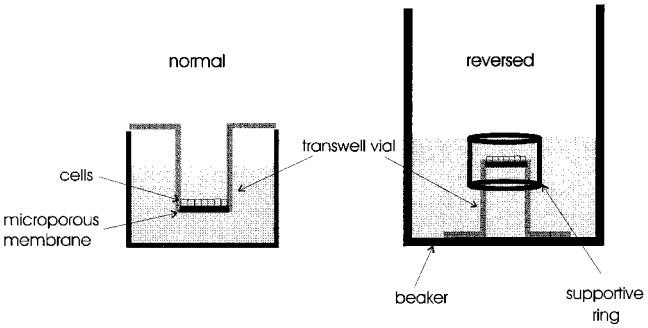

Figure 2—Normal and "reversed" growth of cells on a microporous membrane is illustrated. The left panel shows how cells are normally grown. The transwell vial is hanging in a 24-well plate well, and the cells are grown at the inside of the transwell vial. The right panel shows the "reversed" growth. Now the transwell vial is turned upside down and is completely immersed in growth medium. A polyethylene ring is placed over the transwell vial creating a compartment in which cells can be seeded.

vial. Transport experiments were performed in medium A with 1% FCS. Medium A is a phosphate-buffered saline (PBS) based medium supplemented with essential amino acids for MEM (Flow) with 5.5 mM glucose, 4 mM L-glutamine, and 20 mM HEPES, without bicarbonate (pH 7.4). To remove dust particles, which gave extra background noise during the transport measurements, the medium was filtered (0.22 μm, Millipore).

The detection was most sensitive when fluorescent compounds were added to the transwell vial (upper compartment), and the appearance of the substrate was monitored in the cuvette (the lower compartment). To measure transport from the apical to the basolateral side of the cells (A to B), cells were seeded in the transwell insert. After attachment and growth of the cells, with the basolateral side facing the microporous membrane, the transwell vial was suited to measure transport from A to B. To measure the reversed process, transport from B to A, cells were grown "reversed", at the opposing side of the microporous membrane. In Figure 2 the difference between both ways of growing the cells is illustrated. Before seeding, the transwell was placed in a beaker filled with ±15 mL of growth medium. The transwell was placed upside down, in such a way that there was no air present under the membrane. Then a plastic (polyethylene) supportive ring, which loosely fitted the transwell, was placed around the transwell and approximately 5000 cell/mm^2 were brought within the supportive ring. After 1 day the supportive ring was removed, and confluency was checked by measuring the TER.

Transepithelial Efflux Experiments and Calculations—Just before the start of the transepithelial transport experiment the cells were washed with medium A (at 37 °C), and the growth

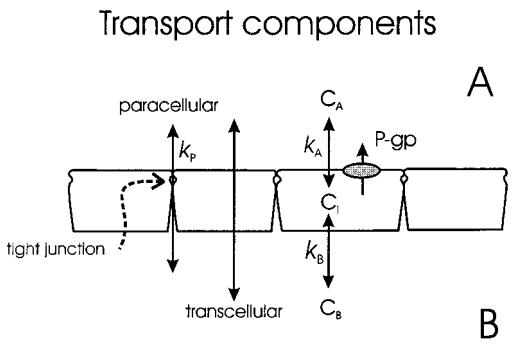

Figure 3—Schematic presentation of an epithelial cell monolayer and the different transport components. Tight junctions are indicated. Pgp is localized in the apical plasma membrane and is modeled using Michaelis–Menten kinetics. The free substrate concentrations in the different compartments are defined as C_A, the apical compartment concentration; C_i, the intracellular concentration; and C_B, the basolateral compartment concentration. Passive plasma membrane transport across the apical membrane is dependent on C_A and C_i and proceeds with a first-order rate constant k_A. Similarly, passive transport across the basolateral membrane takes place, depending on C_B and C_i, and proceeds with a first-order rate constant k_B.

medium was replaced by medium A supplemented with 5% FCS and antibiotics. Then the transwell vial was placed in the cuvette, and the fluorescent substrate was added to the transwell vial. The fluorescence in the cuvette was measured on a computer-controlled fluorometer (FluoroMax, SPEX Industries, Edison, NJ) at excitation and emission wavelengths of 480 and 590 nm for DNR and IDA and 480 and 525 nm for Cal and FITC-dextran. At the end of the experiment both the cells (with 25 μM digitonin) and the microporous membrane (mechanically) were disrupted, and then the equilibrating fluorescence (F_{eq}) was measured, which was used for calibration. The normalized fluorescence (F_n) was calculated according to $F_n = (F - F_b)/(F_{eq} - F_b)$, with F = measured fluorescence and F_b = background fluorescence. From this normalized trace, representing the normalized increase in fluorescence in time ($\Delta F_n/\Delta t$), the flux (J) in pmol/min·cm^2 was calculated using $J = (\Delta F_n/\Delta t)C_T V_T V_C(V_T + V_C)^{-1}A^{-1}$, in which C_T = the applied concentration at the start of the experiment; V_T = volume of the medium in the transwell vial; V_C = volume of the medium in the cuvette; A = surface (0.33 cm^2). (Note: the substrate is diluted in V_C ($V_C \gg V_T$), and therefore backflux from the cuvette compartment is neglected.) Dividing J by C_T gives the permeability (k) (length·time^{-1}).[17] Alternatively, the permeation coefficient (volume·time^{-1}·number of cells^{-1}) may be calculated when reference is made to the amount of cells instead of surface.[23,24]

Octanol/Water Partition Coefficient—The octanol/water partition coefficient is the ratio of the anthracycline concentration in the octanol phase divided by that in the water (= phosphate-buffered saline (PBS)) phase at equilibrium. The ratio was determined at ambient temperature (20−25 °C), by adding 750 μL octanol to 750 μL of a 10 μM anthracycline solution prepared in PBS (pH 7.3). The two phases, which do not mix, were then vigorously shaken for 1 min and centrifuged to separate both phases again. Aliquots of 25 μL of both phases were separately dissolved in 150 μL ethanol (70% solution in water) in a 96-well plate. To obtain an equal medium composition in all the wells, 25 μL PBS was added to the wells containing the 25 μL octanol anthracycline solution, and 25 μL octanol was added to the wells containing the PBS anthracycline solution. The fluorescence of the plate was determined on a Spectrafluor plate reader (Tecan, Austria), using an excitation filter of 492 nm and an emission filter of 595 nm. After background correction, the octanol/water partition coefficient was calculated by the fluorescence of the octanol phase divided by the fluorescence of the water phase.

A Model for Transepithelial Drug Transport—A biomathematical transport model was developed to describe transepithelial transport and the effect of Pgp inhibition by SDZ PSC 833 for transepithelial drug transport from A to B and vice versa. Figure 3 shows a schematic presentation of epithelial cells, with C_A = the apical compartment concentration; C_i = the intracellular concentration; and C_B = the basolateral compartment concentration. The paracellular flux is the concentration in the transwell vial times the paracellular permeation coefficient k_p (per unit surface). The passive plasma membrane flux over the apical membrane is the difference between C_A and C_i times the passive permeation coefficient of the apical membrane k_A (per unit surface). Similarly, the passive flux across the basolateral membrane is the difference between C_B and C_i times the passive permeation coefficient of the basolateral membrane k_B (per unit surface). Pgp is expressed at the apical side of the cell. The Pgp-mediated transport rate (v_{Pgp}) is supposed to follow Michaelis–Menten kinetics:

$$v_{Pgp} = \frac{V_{max} C_i}{K_M + C_i} \tag{1}$$

with K_M = the Michaelis constant and V_{max} = the maximum transport rate. When $C_i \ll K_M$, eq 1 can be simplified to

$$v_{Pgp} = \frac{V_{max}}{K_m} C_i \tag{2}$$

For the transport from A to B, $R_{A\rightarrow B}$ is defined as the transepithelial flux after inhibition (J_{-Pgp}) divided by the transepithelial flux before inhibition (J_{+Pgp}):

$$R_{A\rightarrow B} = \left(\frac{J_{-Pgp}}{J_{+Pgp}}\right)_{A\rightarrow B} \tag{3}$$

At quasi-steady-state (either with or without Pgp transport), the flux across the apical membrane (= $C_o k_A - C_i k_A$) equals the flux across the basolateral membrane (= $C_i k_B$) and $R_{A\rightarrow B}$ can be described in terms of the fluxes across the basolateral membrane plus the paracellular flux. Then eq 3 becomes

$$R_{A\rightarrow B} = \frac{C_i k_B + C_A k_p}{C_i' k_B + C_A k_p} \tag{4}$$

with C_i = the free intracellular concentration in the presence of SDZ PSC 833 and C_i' = the free intracellular concentration in the absence of SDZ PSC 833. (Note that since DNR is strongly diluted in the cuvette compartment the backflux into the cells is neglected.)

In the quasi-steady-state ($dC_i/dt = 0$) the intracellular concentration is constant and is determined by the influx from the apical compartment and the efflux out from the cellular compartment, which gives

$$0 = C_A k_A - C_i' k_A - C_i'\left(\frac{V_{max}}{K_M}\right) - C_i' k_B \tag{5}$$

The possibility that the "unstirred" cytosol acted as an additional barrier was neglected. Based on Fick's first law of diffusion, a diffusion coefficient at 37 °C of 4×10^{-6} cm^2/s, and an average diffusion path length of 5×10^{-6} m, it can be calculated that for the examples mentioned the cytosol forms less than 5% of the total resistance (= the reciprocal permeability) of the cell monolayer. When eq 5 is rewritten, the equation for the intracellular concentration evolves to:

$$C_i' = \frac{C_A}{1 + \frac{k_B}{k_A} + \left(\frac{V_{max}}{K_M k_A}\right)} \tag{6}$$

Equation 6 gives the equation for the intracellular concentration when Pgp is active. When Pgp is inactive ($V_{max} = 0$), the last term in the denominator is zero. Substitution into eq 4 and dividing by ($C_A k_B$) gives the equation for the SDZ PSC 833 induced slope change in terms of k_A, k_B, k_p, and V_{max}/K_M:

$$R_{A\rightarrow B} = \frac{\left[1 + \frac{k_B}{k_A}\right]^{-1} + \frac{k_p}{k_B}}{\left[1 + \frac{k_B}{k_A} + \left(\frac{V_{max}}{K_M k_A}\right)\right]^{-1} + \frac{k_p}{k_B}} \tag{7}$$

An equation for $R_{B\rightarrow A}$, defined as the flux without SDZ PSC 833

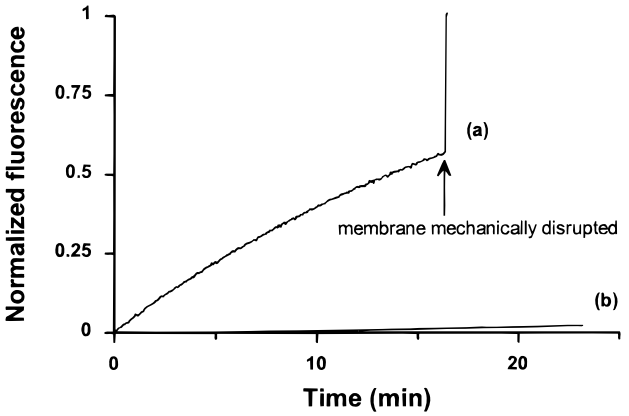

Figure 4—DNR (2 μM) transport from the upper to the lower (cuvette) compartment (a) without cells and (b) with MDCKII cells grown on the microporous membrane.

divided by the flux with SDZ PSC 833, can be derived in a similar way as was done for $R_{A\rightarrow B}$. $R_{B\rightarrow A}$ is given by

$$R_{B\rightarrow A} = \frac{k_B(C_B - C_i') + C_B k_p}{k_B(C_B - C_i) + C_B k_p} \quad (8)$$

C_i and C_i' are now given by

$$C_i' = \frac{C_B}{1 + \frac{k_A}{k_B} + \left(\frac{V_{max}}{K_M k_B}\right)} \quad (9)$$

Substitution of eq 9 into eq 8 gives the equation for $R_{B\rightarrow A}$:

$$R_{B\rightarrow A} = \frac{\left[1 + \left(\frac{V_{max}}{K_M k_A}\right)\right]\left[1 + \frac{k_A}{k_B} + \left(\frac{V_{max}}{K_M k_B}\right)\right]^{-1} + \frac{k_p}{k_A}}{\left[1 + \frac{k_A}{k_B}\right]^{-1} + \frac{k_p}{k_A}} \quad (10)$$

Results and Discussion

Transport with and without Cells on the Microporous Membrane—Figure 4 shows the transport of daunorubicin (DNR) with and without cells present in the transwell vial. Without cells the DNR transport is much faster than with cells on the microporous membrane. Without cells on the membrane, the influence of stirring or not stirring of the upper compartment was clearly reflected in the transport rate after turning the stirrer on and off (data not shown). With cells on the membrane this effect was hardly visible for DNR transport, indicating that diffusion in the transwell compartment was not limiting for the transepithelial transport of DNR. To ensure good mixing of a broad range of compounds, the medium was always gently stirred.

After adding DNR to the transwell compartment with cells on the membrane, a lag time of approximately 30 min was first observed. Thereafter the transport rate became virtually constant. During the lag time, the intracellular free DNR concentration increases until the cellular influx of DNR equals the cellular efflux from the cells. When this is the case, both the transepithelial transport and intracellular free drug concentration stay constant and are at quasi-steady-state. For the DNR transport in wild-type and MDR1 cDNA transfected MDCKII-MDR1 cells, this quasi-steady-state continued for at least 2 h. From $\Delta F_n/\Delta t$ (see Figure 4) at quasi-steady-state the permeation coefficient in cm/min was determined (see Experimental Section). For the DNR transport from A to B the transepithelial permeation coefficients were 0.67 ± 0.05 ($\times 10^{-3}$) cm/min for the wild-type MDCKII cells and 0.44 ± 0.3 ($\times 10^{-3}$) cm/min for the MDCKII-MDR1 cells (Table 1). The increased expression of Pgp in the apical[25] membranes of the MDCKII-MDR1 cells, after transfection of wild-type cells with the MDR1 cDNA, led to a lower A to B transepithelial transport rate compared to the untransfected MDCKII cells (due to backward pumping to A).

Table 1—Transepithelial Transport for MDCKII-MDR1 Cells

	Direction	MDCKII-MDR1 ($\times 10^{-3}$) cm/min	MDCKII ($\times 10^{-3}$) cm/min
DNR	A to B	0.44 ± 0.3[a]	0.67 ± 0.05
Cal	A to B	0.17 ± 0.01	0.04, 0.07
FITC-dextran	A to B	0.04 ± 0.02	0.02, 0.01

[a] Data are given as the mean ± SD of at least three experiments or stated otherwise.

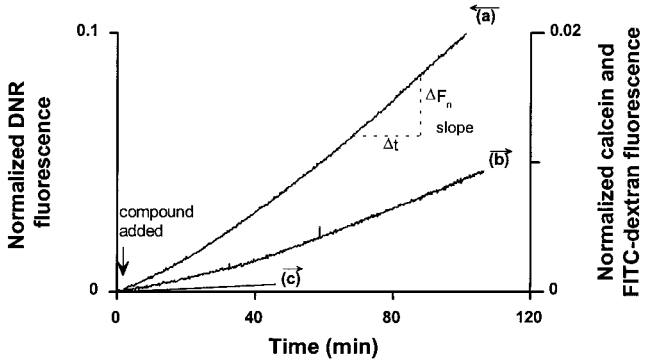

Figure 5—Comparison of (a) DNR (2 μM), (b) Cal (0.4 μM) and (c) FITC-dextran (8 μM) transport across MDCKII wild-type cells grown on microporous membranes. Fluorescent compounds were added to the upper compartment, and transport from the apical to the basolateral side of the cells was measured by monitoring the fluorescence in the cuvette. Representative traces are shown.

Paracellular Transport—To investigate the tightness of the monolayers, the transport of the plasma membrane permeable DNR was compared with that of highly plasma-membrane-impermeable compounds. Figure 5 shows the A to B transport of the organic anion calcein (Cal), the bulky compound FITC-dextran (70 kDa), and DNR for the MDCKII cells. Table 1 presents the transepithelial permeation coefficients for the wild-type and the MDCKII-MDR1 cells for the transport from A to B. The transepithelial transport of Cal for the MDCKII-MDR1 cells is approximately 4 times faster than for the wild-type cells. For FITC-dextran the transepithelial permeation for the wild-type cells was approximately 2 times slower. Why there are these differences between the two lines is not clear. It cannot be explained by differences in TER values of the batches of cells that were used since these were comparable. Possibly components cotransfected or the MDR1 gene itself causes this difference in the epithelial permeability. More certainty about this may be obtained by a detailed mechanistic study, but this does not lie within the scope of this study.

To show the tightness of the cell monolayer, the effect of opening the tight junctions by the calcium chelator EDTA[8,27] was studied. Figure 6 shows the effect of EDTA on the transepithelial transport of FITC-dextran. After a constant flux was observed, EDTA was added as indicated in the figure. A lag time of ~15 min after the EDTA addition was observed, and then the increased transport rate became constant. The inset shows transepithelial transport during the transition from closed to opening of the tight junctions in more detail.

From the constant fluxes before and after addition of EDTA, transepithelial permeation coefficients were calculated. Table 2 gives the transepithelial permeation coef-

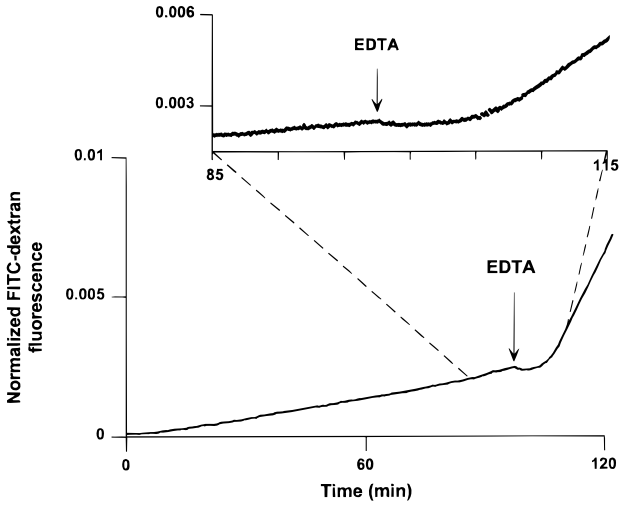

Figure 6—The effect of binding the extracellular calcium with EDTA (2 mM) on the transport FITC-dextran (8 μM) across MDCKII-MDR1 cells. FITC-dextran was added to the upper compartment, and the transport from the apical to the basolateral side of the cells was measured by monitoring the fluorescence in the cuvette. The inset shows the transition from closed to open tight junctions in more detail (85 to 115 min). The traces are representative for at least three experiments.

Table 2—Permeation Coefficients: The Effect of Opening of the Tight Junctions (TJ) for MDCKII-MDR1 Cells

	direction	control[b] ($\times 10^{-3}$) cm/min	TJ open with EDTA[b] ($\times 10^{-3}$) cm/min	R_{TJ}[c]
DNR	B to A	0.8 ± 0.4[a]	2.9 ± 1.0	5.3 ± 2.6
IDA	B to A	1.6 ± 0.2	2.1, 2.9	1.3, 1.7
DNR	A to B	0.7 ± 0.3	4.0 ± 1.1	5.3 ± 1.7
IDA	A to B	2.2 ± 0.9	2.4, 2.9	0.9, 1.1
FITC-dextran	both	0.04 ± 0.02	0.5 ± 0.2	13.1 ± 4.7

[a] Data are given as the mean ± SD of at least three experiments or stated otherwise. [b] SDZ PSC 833 (5–20 μM) was present to inhibit Pgp. [c] Please note that R_{TJ} cannot be derived from the first two columns, because R_{TJ} was calculated from individual (paired) data.

ficients for FITC-dextran, DNR, and IDA for the transport from A to B and vice versa, both in the presence and absence of EDTA. DNR and IDA were used because they are highly similar in chemical structure, but differ in lipophilicity. The difference in lipophilicity was measured by their octanol/water partition coefficient. The partition coefficients were 16.6 ± 0.2 for IDA (mean ± SEM; n =3) and 4.9 ± 0.1 for DNR. The IDA transepithelial transport in the presence of SDZ PSC 833 was a factor 2−3 larger than that of DNR, reflecting the difference in lipophilicity. In all tested cases the permeability increased after addition of EDTA. This increase of the paracellular transport component is expected to be independent of the lipophilicity. It therefore reduces the relative difference between total transport of DNR and IDA through the cellular layer. Measurement of transport from A to B showed a slightly larger permeability for DNR than for IDA. We attribute this to biological variations between cellular layers. To partially avoid effects of these biological variations, the ratio (R_{TJ}) of the fluxes before and after addition of EDTA was calculated within the same experiment. R_{TJ} is presented in Table 2 and decreased in the order FITC-dextran > DNR > IDA. For the hydrophilic compound FITC-dextran the transepithelial flux was strongly dependent on the paracellular route, while for the highly lipophilic IDA, opening of the tight junction hardly influenced the flux, which is in accordance with what can be expected from an increase in lipophilicity (comparing DNR and IDA). This illustrates that the dependence of total transport on the

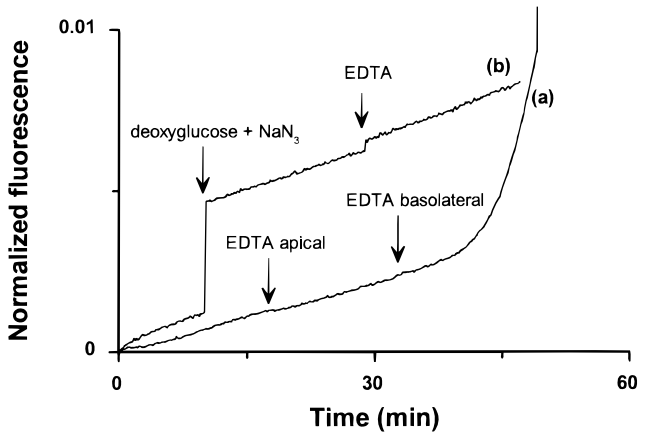

Figure 7—Specificity of the EDTA effect on transepithelial transport of FITC-dextran (8 μM) of MDCKII cells. (a) Effect of adding EDTA apically or basolaterally. As indicated, EDTA (2 mM) was first added to the apical side and then to the basolateral side. (b) Effect of ATP-depletion by the addition of deoxyglucose (6 mM final concentration) and NaN_3 (10 mM final concentration) on the EDTA effect. Deoxyglucose and NaN_3 were added to both the apical and basolateral compartments. Thereafter, EDTA (2 mM) was added (apically and basolaterally). The traces are representative for at least three experiments.

paracellular transport decreases as the lipophilicity/passive membrane permeability increases. From the effects of the tight junctions on the transport, we may conclude that the cell layers stayed intact under the applied conditions. Note that the data presented here were obtained with the MDCKII-MDR1 cells in the presence of SDZ PSC 833 to inhibit Pgp. Similar results were also found for the wild-type MDCKII cells and LLC-PK1[20] cells (data not shown).

Cellular Control of the Tight Junction—The tightness of epithelia and endothelia may be regulated by the cells in order to control the flux of certain molecules (or cells).[8,9] The mechanism by which EDTA triggers the cells to open the paracellular transport route is still under investigation.[6,7,26,28] Extracellular calcium and calcium-dependent protein kinases (PKC) have shown to be directly or indirectly involved in the tight junction tightness.[27,29–31] To show the usefulness of the current method in such regulations studies, we examined (1) the effect of adding EDTA to either side of the monolayer and (2) the influence of ATP-depletion-induced metabolic inhibitors.

Figure 7 (line a) shows the transport of FITC-dextran and the effect of EDTA added to the apical or to the basolateral side. Addition of EDTA to the apical side had no effect. Only when EDTA was present at the basolateral side, then the tight junction opened and an increased FITC-dextran transport was observed. These results are similar to recent observations on the basolateral side specificity of Ca^{2+}.[32,33] Figure 7 (line b) shows the effect of adding an excess of both the nonmetabolizable deoxyglucose (6 mM) and the respiratory inhibitor NaN_3 (10 mM), added to both compartments, on the FITC-dextran transport. It can be seen that addition of NaN_3/deoxyglucose caused an instant increase in the background fluorescence, which may be related to the yellowish color. Looking at the fluxes, it can be seen that the ATP-depletion itself did not affect the FITC-dextran transport rate. However, under these conditions EDTA did not open the tight junctions anymore. Similar results were also obtained for LLC-PK1 cells both measuring the transepithelial transport and measuring the TER (data not shown). This strongly suggests that the effect of EDTA on the tight junctions is ATP-dependent and most probably involving ATP dependent phosphorylation mechanisms.[31,34–36] However, at this point we cannot exclude direct interactions between deoxyglucose or NaN_3

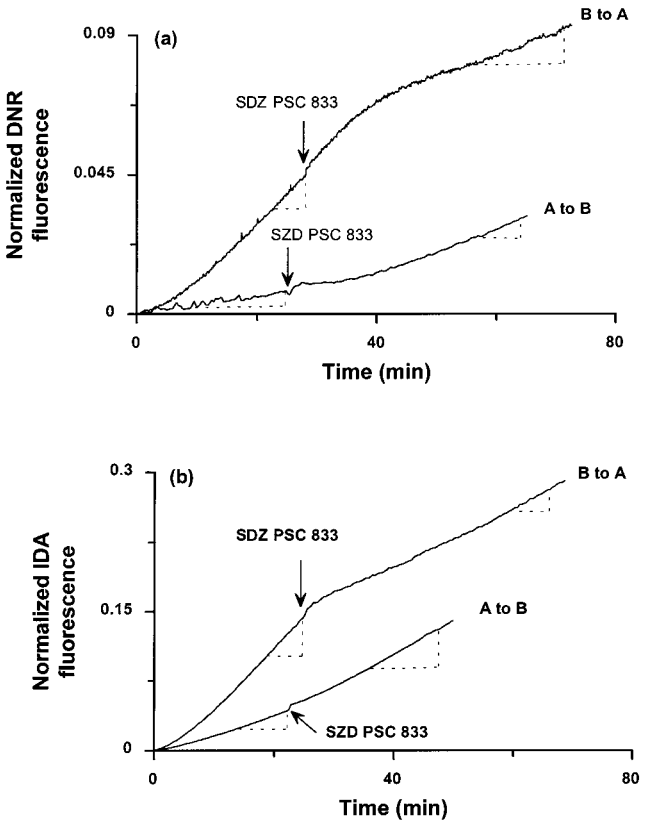

Figure 8—SDZ PSC 833 modulation of (a) the DNR (2 μM) and (b) the IDA (2 μM) transepithelial transport across MDCKII-MDR1 cells. The effect of SDZ PSC 833 was measured for the transport from A to B and from B to A, as indicated. After reaching the quasi-steady-state, SDZ PSC 833 (5–20 μM) was added to the cells to inhibit Pgp. The traces are representative for at least three experiments.

and EDTA. These experiments show that our system can be useful for further elucidating mechanisms of paracellular transport. This application shows that the method can be useful to study (1) compounds that diffuse rapidly (e.g., when the tight junctions are open) and (2) modulators that induce rapid changes (in the minute time range) in the transepithelial transport.

Effect of Pgp on Transepithelial DNR and IDA Transport—The apical localization of Pgp results in a decreased flux from A to B and an increased flux from B to A. Consequently, inhibition of Pgp will lead to an increase in transepithelial flux from A to B and to a decrease from B to A. To be able to perform experiments in which Pgp can be modulated, three Pgp inhibitors, verapamil (Vp), diltiazem (Dil), and SDZ PSC 833, were tested for their effect on the paracellular transport of FITC-dextran across MDCKII-MDR1 cells. At concentrations needed to rapidly inhibit Pgp, Dil (>0.5 mM) and Vp (>200 μM) increased the FITC-dextran transport (not shown). Pgp inhibitor SDZ PSC 833 (1−25 μM) did not influence the FITC-dextran (and Cal) transport and was used for further study of the effect of Pgp inhibition on the transepithelial transport of DNR and IDA. Figure 8 shows the transepithelial transport using the MDCKII-MDR1 cells for DNR (Figure 8a) and IDA (Figure 8b) for transport from A to B and vice versa. After the quasi-steady-state was reached, the effect of Pgp inhibition was measured by adding SDZ PSC 833 (5 μM) to both compartments, as is indicated in Figures 8a and 8b. The addition of SDZ PSC 833 to the cuvette gave rise to an increase of the background fluorescence, due to the weak fluorescence of SDZ PSC 833. In later experiments it was found that addition of 5−20 μM SDZ PSC 833 only to the transwell compartment was sufficient to inhibit Pgp with a lower disturbance of the background signal. After the addition of SDZ PSC 833, the transepithelial flux changed slowly and stabilized after approximately 30 min. In the case of A to B transport, the flux increased, and in the case of B to A transport, the flux decreased (Figure 8; Table 3). From the fluxes at quasi-steady-state, the transepithelial permeation coefficients were calculated, which are presented in Table 3. To be able to compare the effect of Pgp inhibition for the different compounds, the effect of SDZ PSC 833 was quantified by the ratio of the fluxes before and after Pgp inhibition. This ratio was called the SDZ PSC 833-induced slope change (R). To be able to compare R for the transport from A to B and vice versa, the R was defined as the larger slope divided by the smaller slope. Table 3 shows the obtained SDZ PSC 833-induced slope changes. For FITC-dextran, addition of SDZ PSC 833 did not lead to change in the flux. For IDA and DNR, addition of SDZ PSC 833 led to changes in the transepithelial fluxes. Moreover, it was found that for both IDA and DNR the effect of Pgp inhibition was largest for the transport from B to A.

Table 3.—Permeation Coefficients: the Effect of SDZ PSC 833-Induced Pgp Inhibition for MDCKII-MDR1 Cells

	direction	control ($\times 10^{-3}$) cm/min	with SDZ PSC 833 ($\times 10^{-3}$) cm/min	R[b]
DNR	B to A	2.6 ± 1.0[a]	0.8 ± 0.4	3.7 ± 1.4
IDA	B to A	3.8 ± 1.3	1.6 ± 0.2	2.4 ± 0.6
DNR	A to B	0.44 ± 0.3	0.7 ± 0.3	1.6 ± 0.5
IDA	A to B	1.4 ± 0.5	2.2 ± 0.9	1.5 ± 0.2
FITC-dextran	both	0.04 ± 0.02	0.04 ± 0.02	1.1 ± 0.3

[a] Data are given as the mean ± SD of at least three experiments. [b] Please note that R cannot be derived from the first two columns, because R was calculated from individual (paired) data.

Comparison of Experimental Data with the Model—To seek an explanation for the difference in effects of SDZ PSC 833 on the transport from A to B and vice versa, a biomathematical transport model was developed (see Experimental Section). Figure 3 shows a schematic presentation of an epithelial monolayer. Using eqs 7 and 10, which describe R for transport from A to B ($R_{A\rightarrow B}$) and from B to A ($R_{B\rightarrow A}$), respectively, the theoretical differences between the transport from the A to B and transport vice versa were studied for nonsaturating conditions. Figure 9a shows a simulation of the relationship between R and the Pgp concentration ($\sim V_{max}/(K_M k_A)$). In this simulation the passive permeation coefficients were kept constant and equal. The figure shows a linear relationship between the Pgp concentration and $R_{A\rightarrow B}$. A nonlinear relationship was found for $R_{B\rightarrow A}$. In the lower range ($V_{max}/(K_M k_A) \ll 1$) $R_{B\rightarrow A}$ increases almost linearly with increasing Pgp concentration. At values of $V_{max}/(K_M k_A) > 1$, $R_{B\rightarrow A}$ goes to a plateau and Pgp loses control over the transepithelial flux. The latter can be explained by the high Pgp activity, resulting in C_i values approaching zero and the basolateral membrane getting more and more in control of the transcellular flux. In the extreme case Pgp completely clears the cell of almost all drug, while the transcellular flux becomes equal to the flux across the basolateral membrane ($= C_B k_B$). When also paracellular transport is taking place, R decreases (dashed lines Figure 9a) and $R_{A\rightarrow B}$ seems to be more affected by the paracellular flux than $R_{B\rightarrow A}$. The simulations in Figure 9a show that in general one may expect that Pgp has a higher control over the transport from A to B than vice versa, which seems in contradiction with our experiments. However, k_B and k_A may not be equal for these cells. Figure 9b shows the relationship between k_B/k_A and both $R_{B\rightarrow A}$ and $R_{A\rightarrow B}$. At low ratios of k_B/k_A, $R_{A\rightarrow B}$ is larger than $R_{B\rightarrow A}$; however, at higher ratios of k_B/k_A (>2)

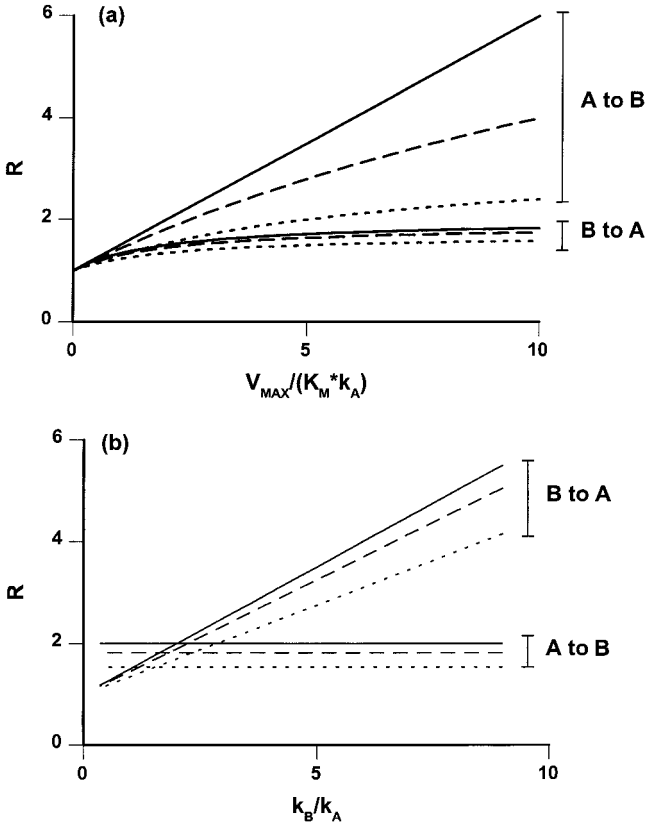

Figure 9—Simulations of the SDZ PSC 833-induced slope change for the transport from A to B and from B to A. In (a) Pgp was varied by changing the dimensionless factor $V_{max}/(K_M k_A)$, while k_A and k_B were both kept constant at 6.25×10^{-3} cm/min. These relative estimates correspond to those of moderately multidrug resistant cells.[21] (b) Simulation of the dependence R on the ratio of the basolateral over the apical membrane permeation coefficient (k_B/k_A). V_{max}/K_M was kept constant at 12.5×10^{-3} cm/min; ($k_B + k_A$) was set at 12.5×10^{-3} cm/min, and the ratio k_B/k_A was varied. In both a and b three conditions are shown: (1) when there is no paracellular transport (solid lines); (2) when the paracellular permeability is 10% (long dashes); (3) 30% (short dashes) of the total transepithelial permeability.

the situation is reversed and $R_{B\to A}$ becomes larger than $R_{A\to B}$. When the paracellular transport of DNR and IDA are approximately equal to the transepithelial transport of Cal, then the paracellular transport will make up 10−30% of the total transepithelial transport of DNR and IDA. Introducing a paracellular flux in the model leads to an overall decrease of the ratios (dashed lines Figure 9b). However, the crossing of the lines for $R_{A\to B}$ and $R_{B\to A}$ occurs at approximately the same k_B/k_A (range 1.6−2). At $k_B > 2k_A$ the model predicts similar results as found in the experiments. Although the relations plotted in Figure 9b still are dependent on the V_{max}/K_M, the passive membrane permeabilities, and the paracellular permeability, these results show that for both DNR and IDA, $k_B > k_A$. On the basis of our transport data for DNR and IDA, k_B will be approximately 3−7 times larger than k_A, and this estimate tends to be larger for DNR than for IDA. This difference could be due to the differences in passive membrane permeation coefficients (Figure 9a).

An explanation for the larger k_B may be a larger basolateral membrane than apical membrane surface. The simplest model of a cell is a cube, with the tight junction localized to the top rim of the cells, with 1/6 of the membrane localized apically and 5/6 localized basolaterally. However, most epithelial cells contain microvilli at their apical side and basolateral clefts at their basolateral side, making it more complicated to compare both surface areas. A low number of microvilli when compared to basolateral clefts may also explain our observation. However, different compositions in lipids or proteins of the apical and basolateral membranes may also explain such differences in membrane permeabilities. For instance basolaterally located transport proteins, like the organic cation transporter (Oct1),[37] may increase the basolateral transport for neutral as well as for the protonated[38] form of DNR and IDA. Recent studies have shown that such transport proteins may be involved in the basolateral uptake of organic cations and are present in renal cell lines.[39]

In summary, we present here a new method to measure the transepithelial transport of fluorescent compounds online and at (sub)minute time resolution. It makes use of commercially available plasticware and a fluorometer, equipment present in most biochemical laboratories. It is simple to perform and relatively inexpensive. To reduce the influence of stagnant layers[17] on the transport, the media in both the apical and basolateral compartments can be continuously stirred and thermostated. We have shown that both paracellular and transcellular transport and modulation of both types of transport can be studied. Moreover, the paracellular transport studies showed that the monolayer stayed intact during the experiments (up to 4 h) and was not disrupted by the stirring of the medium, which was confirmed by microscopy (not shown). Related to this point we like to bring up that when the cell monolayer was already leaky at the beginning of the experiment (less than 5% of the cases) this became directly evident from the transport that was observed. Thus the method allowed us to terminate and discard such experiments. Comparing the fluorescent compounds DNR, IDA, Cal, and FITC-dextran, we found the highest transepithelial transport rate for the highly membrane-permeable IDA and the lowest for bulky and membrane-impermeable FITC-dextran. Site specificity for the EDTA-induced opening of the tight junctions was bound to basolateral side of the cells, which has also been reported by other groups.[32,33] Moreover, we found that adding an excess of metabolic inhibitors could inhibit the effect EDTA on the tight junctions. These experiments show that the method can be useful to study paracellular transport. For the transepithelial transport of DNR and IDA with the MDCKII-MDR1 cells, we found that Pgp inhibition was most effective for transport form B to A. Modeling showed that this was possible at $k_B > 2k_A$. We estimated that k_B was approximately 3−7 larger than k_A. The biomathematical transport model showed that the effect of Pgp on the transepithelial transport is dependent on the Pgp concentration and on the ratio of k_B/k_A. At higher Pgp concentrations and at lower ratios of k_B/k_A, Pgp gets more control over the A to B transepithelial transport, but loses control over the B to A transport. Extrapolation of these results to the in vivo situation of patients receiving anticancer drugs such as DNR or other Pgp-interacting drugs suggests that decreased efflux from the blood or increased influx from the lumen of the gut by treatment with Pgp modulators can differ quantitatively, depending on the contribution of transport components for uptake and efflux across the apical or basolateral membrane. Where there is a basolaterally localized uptake system involved in the transport, it may be worthwhile to inhibit this transport, thereby indirectly reducing the Pgp-mediated excretion. Moreover, inhibition of Pgp after an intravenous bolus injection of Pgp substrate drugs may lead to unexpected differences in clearance from the blood and uptake into the brain, depending on the (passive) permeation properties of the drug that is used. Using the method described here, one may study these properties in greater detail and so may understand and predict the in vivo situation better.

References and Notes

1. Topp E. M. Barriers to delivery of macromolecules. *Med. Chem. Res.* **1997**, *7*, 493−508.
2. Hayashi M.; Tomita M.; Awazu S. Transcellular and paracellular contribution to transport processes in the colorectal route. *Adv. Drug Deliv. Rev.* **1997**, *28*, 191−204.
3. Lennernas H. Human intestinal permeability. *J. Pharm. Sci.* **1998**, *87*, 403−410.
4. Staddon J. M.; Rubin L. L. Cell adhesion, cell junctions and the blood-brain barrier. *Curr. Opin. Neurobiol.* **1996**, *6*, 622−627.
5. Cereijido M.; Valdes J.; Shoshani L.; Contreras R. G. Role of tight junctions in establishing and maintaining cell polarity. *Annu. Rev. Physiol.* **1998**, *60*, 161−177.
6. Mitic L. L.; Anderson J. M. Molecular architecture of tight junctions. *Annu. Rev. Physiol.* **1998**, *60*, 121−142.
7. Spring K. R. Routes and mechanism of fluid transport by epithelia. *Annu. Rev. Physiol.* **1998**, *60*, 105−119.
8. Koepsell H. Organic cation transporters in intestine, kidney, liver, and brain. *Annu. Rev. Physiol.* **1998**, *60*, 243−266.
9. Gottesman M. M.; Hrycyna C. A.; Schoenlein P. V.; Germann U. A.; Pastan I. Genetic analysis of the multidrug transporter. *Annu. Rev. Genet.* **1995**, *29*, 607−649.
10. Germann U. A. P-glycoprotein − A mediator of multidrug resistance in tumour cells. *Eur. J. Cancer* **1996**, *32A*, 927−944.
11. Juliano R. L.; Ling V. A surface glycoprotein modulating drug permeability in Chinese hamster ovary cell mutants. *Biochim. Biophys. Acta* **1976**, *455*, 152−162.
12. Ford J. M. Experimental reversal of P-glycoprotein-mediated multidrug resistance by pharmacological chemosensitisers. *Eur. J. Cancer* **1996**, *32A*, 991−1001.
13. Lee C. G. L.; Gottesman M. M.; Cardarelli C. O.; Ramachandra M.; Jeang K. T.; Ambudkar S. V.; Pastan I.; Dey S. HIV-1 protease inhibitors are substrates for the MDR1 multidrug transporter. *Biochemistry* **1998**, *37*, 3594−3601.
14. Borst P.; Schinkel A. H. Genetic dissection of the function of mammalian P-glycoproteins. *Trends Genet.* **1997**, *13*, 217−222.
15. Schinkel A. H. The physiological function of drug-transporting P-glycoproteins. *Semin. Cancer. Biol.* **1997**, *8*, 161−170.
16. van Asperen J.; Mayer U.; van Tellingen O.; Beijnen J. H. The functional role of P-glycoprotein in the blood-brain barrier. *J. Pharm. Sci.* **1997**, *86*, 881−884.
17. Adson A.; Burton P. S.; Raub T. J.; Barsuhn C. L.; Audus K. L.; Ho N. F. H. Passive diffusion of weak organic electrolytes across Caco-2 cell monolayers: Uncoupling the contributions of hydrodynamic, transcellular, and paracellular barriers. *J. Pharm. Sci.* **1995**, *84*, 1197−1204.
18. Evers R.; Kool M.; van Deemter L.; Janssen H.; Calafat J.; Oomen L. C. J. M.; Paulusma C. C.; Elferink R. P. J. O.; Baas F.; Schinkel A. H.; Borst P. Drug export activity of the human canalicular multispecific organic anion transporter in polarized kidney MDCK cells expressing cMOAT (MRP2) cDNA. *J. Clin. Invest.* **1998**, *101*, 1310−1319.
19. Madara J. L. Regulation of the movement of solutes across tight junctions. *Annu. Rev. Physiol.* **1998**, *60*, 143−159.
20. Mullin J. M.; Soler A. P.; Laughlin K. V.; Kampherstein J. A.; Russo L. M.; Saladik D. T.; George K.; Shurina R. D.; O'Brien T. G. Chronic exposure of LLC−PK1 epithelia to the phorbol ester TPA produces polyp-like foci with leaky tight junctions and altered protein kinase C-alpha expression and localization. *Exp. Cell Res.* **1996**, *227*, 12−22.
21. Wielinga P. R.; Heijn M.; Broxterman H. J.; Lankelma J. P-glycoprotein-independent decrease in drug accumulation by phorbol ester treatment of tumor cells. *Biochem. Pharmacol.* **1997**, *54*, 791−799.
22. Lankelma J.; Spoelstra E. C.; Dekker H.; Broxterman H. J. Evidence for daunomycin efflux from multidrug-resistant 2780AD human ovarian carcinoma cells against a concentration gradient. *Biochim. Biophys. Acta* **1990**, *1055*, 217−222.
23. Wielinga, P. R.; Heijn, M.; Westerhoff, H. V.; Lankelma, J. A method for studying plasma membrane transport with intact cells using computerized fluorometry. *Anal. Biochem.* **1998**, *263*, 221−231.
24. Lankelma J.; Laurensse E.; Pinedo H. M. A flow-through tissue culture system with fast dynamic response. *Anal. Biochem.* **1982**, *127*, 340−345.
25. Bakos, E.; Evers, R.; Szakacs, G.; Tusnady, G. E.; Welker, E.; Szabo, K.; de Haas, M.; van Deemter, L.; Borst, P.; Varadi, A.; Sarkadi, B. Functional Multidrug Resistance Protein (MRP1) Lacking the N-terminal Transmembrane Domain. *J. Biol. Chem.* **1998,** *273*, 32167−32175.
26. Adson A.; Raub T. J.; Burton P. S.; Barsuhn C. L.; Hilgers A. R.; Audus K. L.; Ho N. F. H. Quantitative approaches to delineate paracellular diffusion in cultured epithelial cell monolayers. *J. Pharm. Sci.* **1994**, *83*, 1529−1536.
27. Stuart R. O.; Nigam S. K. Regulated assembly of tight junctions by protein kinase C. *Proc. Natl. Acad. Sci. U.S.A.* **1995**, *92*, 6072−6076.
28. Kovbasnjuk O. N.; Szmulowicz U.; Spring K. R. Regulation of the MDCK cell tight junction. *J. Membr. Biol.* **1998**, *161*, 93−104.
29. Stuart R. O.; Sun A.; Panichas M.; Hebert S. C.; Brenner B. M.; Nigam S. K. Critical role for intracellular calcium in tight junction biogenesis. *J. Cell. Physiol.* **1994**, *159*, 423−433.
30. Tomita M.; Hayashi M.; Awazu S. Absorption-enhancing mechanism of EDTA, caprate, and decanoylcarnitine in Caco-2 cells. *J. Pharm. Sci.* **1996**, *85*, 608−611.
31. Mullin J. M.; Kampherstein J. A.; Laughlin K. V.; Clarkin C. E. K.; Miller R. D.; Szallasi Z.; Kachar B.; Soler A. P.; Rosson D. Overexpression of protein kinase C-delta increases tight junction permeability in LLC−PK1 epithelia. *Am. J. Physiol. Cell. Physiol.* **1998**, *44*, C544−C554.
32. Collaresbuzato C. B.; Mcewan G. T. A.; Jepson M. A.; Simmons N. L.; Hirst B. H. Paracellular barrier and junctional protein distribution depend on basolateral extracellular Ca2+ in cultured epithelia. *Biochim. Biophys. Acta* **1994**, *1222*, 147−158.
33. Lynch R. D.; Tkachukross L. J.; Mccormack J. M.; Mccarthy K. M.; Rogers R. A.; Schneeberger E. E. Basolateral but not apical application of protease results in a rapid rise of transepithelial electrical resistance and formation of aberrant tight junction strands in MDCK cells. *Eur. J. Cell. Biol.* **1995**, *66*, 257−267.
34. Citi S.; Denisenko N. Phosphorylation of the tight junction protein cingulin and the effects of protein kinase inhibitors and activators in MDCK epithelial cells. *J. Cell. Sci.* **1995**, *108*, 2917−2926.
35. Collaresbuzato C. B.; Jepson M. A.; Simmons N. L.; Hirst B. H. Increased tyrosine phosphorylation causes redistribution of adherens junction and tight junction proteins and perturbs paracellular barrier function in MDCK epithelia. *Eur. J. Cell. Biol.* **1998**, *76*, 85−92.
36. Sakakibara A.; Furuse M.; Saitou M.; AndoAkatsuka Y.; Tsukita S. Possible involvement of phosphorylation of occludin in tight junction formation. *J. Cell. Biol.* **1997**, *137*, 1393−1401.
37. Grundemann D.; Gorboulev V.; Gambaryan S.; Veyhl M.; Koepsell H. Drug excretion mediated by a new prototype of polyspecific transporter. *Nature* **1994**, *372*, 549−552.
38. Skovsgaard T.; Nissen N. I. Membrane transport of anthracyclines. *Pharm. Ther.* **1982**, 18, 293−311.
39. Smit J. W.; Weert B.; Schinkel A. H.; Meijer D. K. F. Heterologous expression of various P-glycoproteins in polarized epithelial cells induces directional transport of small (type 1) and bulky (type 2) cationic drugs. *J. Pharmacol. Exp. Ther.* **1998**, *286*, 321−327.

Acknowledgments

We like to thank Drs. Evers and Borst for the gift of the MDCKII-MDR1 cells. This study was supported by the Dutch Cancer Society (KWF grant VU 94-773 to J.L.).

JS980497Z